BMC Oral Health

RESEARCH Open Access

Biomechanical effects of functional clear aligners on the stomatognathic system in teens with class II malocclusion: a new model through finite element analysis

Mingxin Zhang[1†], Xulin Liu[1†], Ruijie Zhang[1], Xin Chen[1], Zhixin Song[1], Yanning Ma[1*] and Zuolin Jin[1*]

Abstract

Objectives The Functional Clear Aligner (FCA) is a novel orthodontic appliance designed for the treatment of Class II malocclusion with mandibular retrognathia in adolescents. The aim of this study was to investigate the biomechanical characteristics of the masticatory muscles, jawbone, and temporomandibular joint (TMJ) during mandibular advancement using either FCA or Class II elastics combined with clear aligner (Class II elastics) through finite element analysis.

Materials and methods A 3D finite element model of the 'muscle-jawbone-TMJ-appliance' system was constructed based on CBCT and MRI images of a boy with skeletal Class II malocclusion. Masticatory muscles included masseter, temporal, medial pterygoid, and lateral pterygoid muscles. The TMJ consists of the temporal bone's glenoid fossa, disc, and mandibular condyle. To observe the biomechanical characteristics of the muscles and TMJ during orthodontic appliance wearing and the retention phase, two different protocols were used: Model 1: The mandibular advancement using FCA; Model 2: The mandibular advancement using Class II elastics.

Results The FCA group produced greater and more coordinated masticatory muscle forces compared to the Class II elastics group. Temporal and masseter muscles exhibited the most pronounced variation in muscle strength during mandibular advancement. The FCA group exhibited greater TMJ region stress compared to the Class II elastics group. Interestingly, the stress on the articular discs in both models decreased over time. Tensile stresses were observed in both the condyle and the posterior region of the articular fossa.

Conclusion During skeletal Class II malocclusion treatment, masticatory muscle forces and stress on the TMJ were higher in the FCA group compared to the Class II elastics group. In both models, stress cushioning was provided by the articular disc.

[†]Mingxin Zhang and Xulin Liu contributed equally to the paper.

*Correspondence:
Yanning Ma
blueskyabc1007@163.com
Zuolin Jin
zuolinj@163.com

Full list of author information is available at the end of the article

Keywords Masticatory muscles, Mandibular advancement, Functional clear aligner, Class II elastics, Finite element analysis

Background

Class II malocclusion, a highly prevalent orofacial deformity [1], has a negative effect on facial aesthetics, oral function, and mental health. Skeletal Class II malocclusion is induced by alterations to the shape, size, proportion, and growth of the bones in the craniomaxillofacial complex, and is accompanied by problems such as deep overbite, deep overjet, masticatory muscle disorders (MMDs) and temporomandibular joint disorders (TMDs). Current findings indicate that more than 60% of skeletal Class II malocclusions are caused by mandibular hypoplasia, with only 10% of patients presenting with sole maxillary protrusion [2]. Therefore, orthodontic treatment with functional appliances is often focused on mandibular advancement.

Traditional functional tools, such as Twin-block, have shown promising results in correcting the sagittal intermaxillary jaw relationship [3]. With the rapid development of digital technology and biocompatible materials, Functional Clear Aligners (FCAs), such as Invisalign MA, Angelalign A6, and Smartee S8 are increasingly being applied in the treatment of patients with skeletal Class II. Similar to Twin-block, FCAs are designed with bimaxillary plates or precision wings on clear aligners to achieve mandibular advancement, reestablish muscle balance, and stimulate mandibular growth [4]. Class II elastics are an alternative method of treating Class II malocclusion. In a systematic review conducted by Guilherme et al. [5], it was found that Class II elastics exhibit comparable long-term effects to those achieved by functional appliances. Interestingly, the principles of these two appliances on the correction of Class II malocclusion are distinct. Nevertheless, the specific effects of these two distinct appliances on the masticatory muscles and temporomandibular joint (TMJ) region during the treatment of Skeletal Class II deformities remain unclear. Finite element analysis (FEA) is a numerical simulation method that has emerged as a useful tool for studying mechanical interaction between tissues. In orthodontic research, FEA has been widely applied in the field of TMJ biomechanics [6, 7]. A previous study on FEA proposed that the masticatory muscles should be segmented into the masseter muscles, the temporal muscles, the medial pterygoid muscles, and the lateral pterygoid muscles [8]. In the present study, we leveraged the modeling approaches of previous studies to optimize and enhance their performance [9]. This study aimed to (1) construct an innovative 3D finite element model of 'muscle-jawbone-TMJ-appliance' system model; (2) simulate the realistic orthodontic appliance wearing process in orthodontics, the orthodontic appliance insertion was divided into a wearing phase (0–0.1 s) and a holding phase (0.1–100 s); (3) analyze and compare the mechanical characteristics of masticatory muscles and TMJ over time using FCAs and Class II elastics.

Materials and methods

Case selection

A 12-year-old male patient presenting with a skeletal Class II division 1 malocclusion and mandibular retrognathia (ANB 7°, incisal overjet of 8 mm) was included in this study. The volunteer and his parents provided informed consent to participate in the study. This study was approved by the Ethics Committee of The Air Force Medical University (No. IRB-REV-2022079).

Finite element model

The geometric model of the craniofacial region was obtained from a cone beam computed tomography (CBCT) scan. The thickness of each CBCT slice was 0.25 mm. The slice increment was 0.25 mm. The number of slices was 623 and the pixel size was 0.25 mm. Because CBCT imaging cannot visualize the masticatory muscles, and disc (due to lack of radiodensity), MRI (GE 0.5T VMX2 Magnet and Cryogen system with Efilm Software) was employed as a complementary imaging technique. The scan data were exported to DICOM image files. Then the DICOM data was imported into the Mimics system (Version 21; Materialize Software, Belgium) for further analysis. When treating Skeletal Class II patients for mandibular advancement, the orthodontist often focuses on modifying the TMJ region and altering the stability of the masticatory muscles [1, 10]. Our study focuses on this as well. The masticatory muscles can be narrowly classified into four pairs, which are the temporal, masseter muscle, medial pterygoid, and lateral pterygoid muscles. It can be subdivided specifically according to its fiber orientation and layers. As shown in Fig. 1, they are the superficial masseter muscle (SM), deep masseter muscle (DM), anterior temporal muscle (AT), medial temporal muscle (MT), posterior temporal muscle (PT), medial pterygoid muscle (MP), superior lateral pterygoid muscle (SLP), and inferior lateral pterygoid muscle (ILP). According to Duggal's FEA study on orthopedic treatment, future research should segment the TMJ region into the condyle, disc, and fossa [11]. The articular disc was meticulously trimmed based on MRI data to align with the anatomical structure. A thin layer of cartilage covers the condylar and mandibular fossa surfaces, facilitating even distribution of contact pressure across the disc. To replicate the corresponding articular cartilage, two layers of uniform thickness were fabricated to cover condylar (1.15 mm) and temporal (0.41 mm) bone articular surfaces, thus emulating

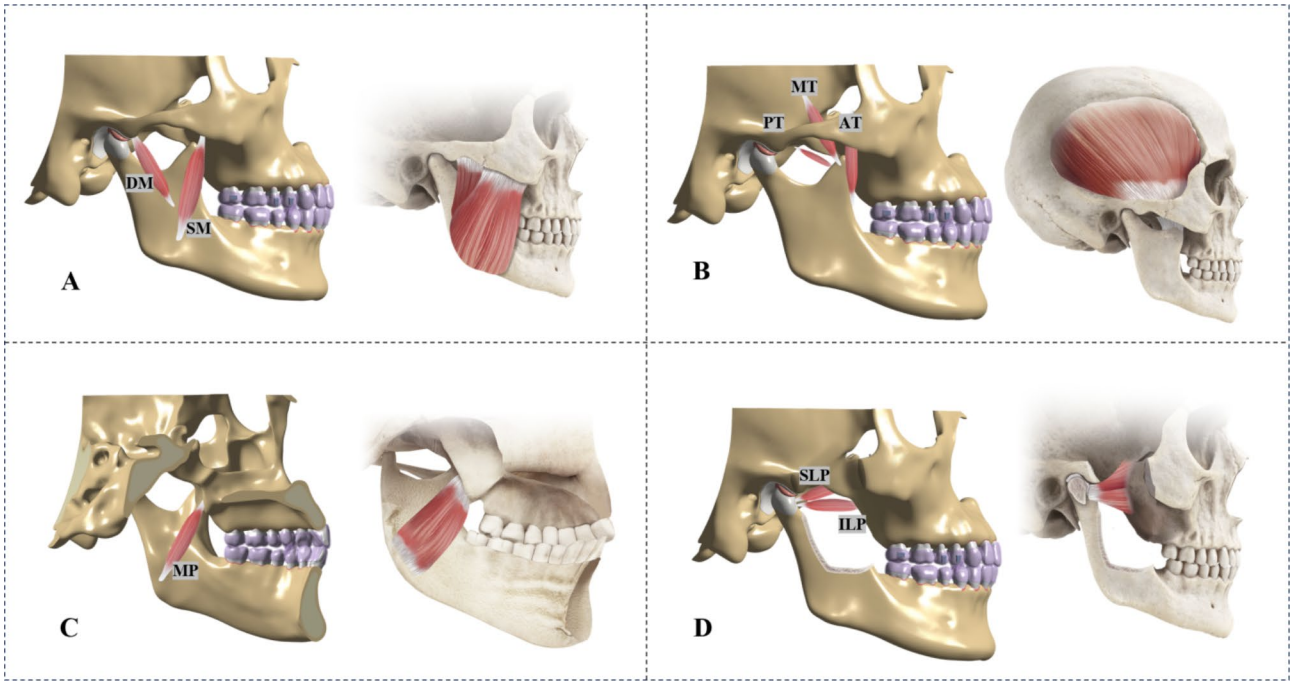

Fig. 1 Schematic diagram about the location and direction of the masticatory muscles. (**A**) SM-Superficial Masseter Muscle, DM-Deep Masseter Muscle; (**B**) AT-Anterior Temporal Muscle, MT-Medial Temporal Muscle, PT-Posterior temporal Muscle; (**C**) MP-Medial Pterygoid Muscle; (**D**) SLP-Superior Lateral Pterygoid Muscle, ILP-Inferior Lateral Pterygoid Muscle

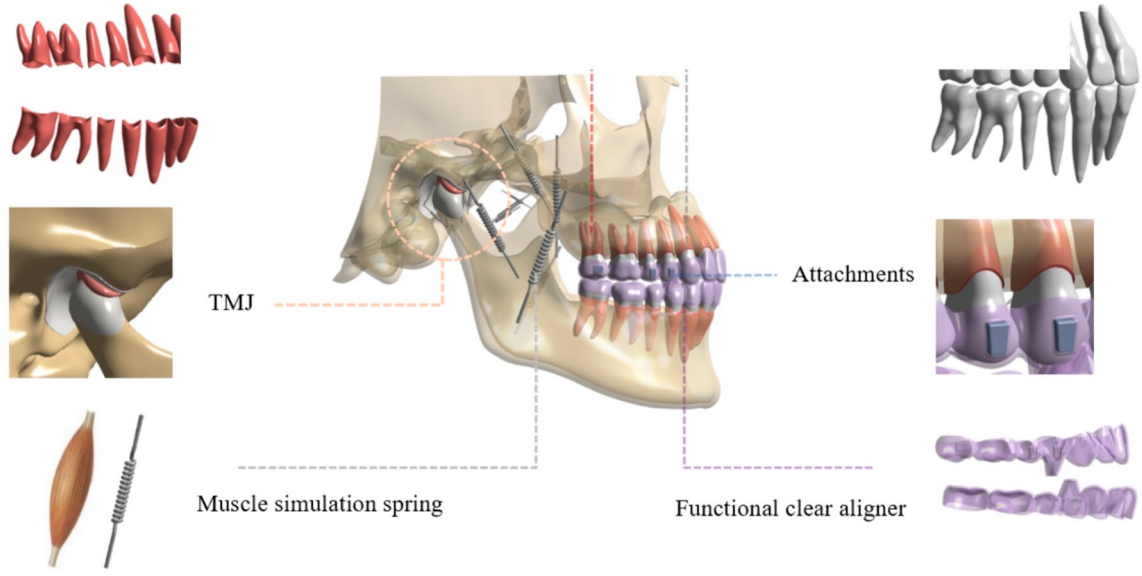

Fig. 2 Configuration of the finite element model simulation

the respective articular cartilages [12]. The maxilla and mandible were moved inwards by 1.3 mm using the offset command and then cortical bone and cancellous bone models were established by Boolean subtraction operation instructions.

Precision cutting on the labial surface of the maxillary canine was chosen as the fixation method for the Class II elastics in this study. For retention purposes, a conventional vertical rectangular attachments (2×3×1 mm) were designed on the buccal surface of maxillary premolars, and a horizontal rectangular attachment (3×2×1 mm) was designed on the upper maxillary second molar. As shown in Fig. 2, the tooth crowns and attachments were extended outward by 0.5 mm in order to simulate a clear aligner appliance [13].

The two sets of models (Fig. 3) were created to simulate a simplified process of mandibular advancement using different orthodontic appliances. Model 1 simulated the use of an FCA, whereas Model 2 imitated the use of a clear aligner combined with Class II elastics. Model 1 was designed with double occlusal plates on clear aligners in the upper and lower regions of the first premolar. The bite block angle was designed to be 70°. Model 2 was constructed by combining clear aligners with Class II elastics using a button on the mandibular first molar and a precision cut on the maxillary canine. For the maxillary canine, corresponding sections of the clear aligner were removed to create attachment points.

Mesh partitioning

All components were imported into ANSYS Workbench 2019 (Ansys, USA) to construct an appropriate 3D Finite Element-based model for finite element analysis. After smoothing and filtering procedures, meshes were created using the discretization method. The quality of the mesh has a significant influence on the convergence of the analysis results, hence, we controlled the mesh quality during division. We experimented with three distinct mesh designs, and the precise mesh assignments were listed in Table 1. Theoretically, the finer mesh, the more accurate the result, but the increase in the number of grid elements, will lead to an increase in the amount of computation, and the requirements for hardware will be higher. Therefore, we tried to optimize the grid under the conditions of existing hardware, so that the number of grid elements is within a reasonable range, and at the same time, the accuracy of the calculation will not be lost. After performing a convergence analysis of the mesh (Fig. 4.), we finally chose the group B mesh design, i.e. alveolar bone is 4 mm, the periodontal ligament (PDL) is 1 mm, the attachment is 0.5 mm, the tooth is 2 mm, the clear aligner is 2 mm, the disc is 1 mm, and the cartilage is 1 mm (Fig. 5. A). The reconstructed detailed anatomical pattern of the TMJ area is displayed in Fig. 5. B. The meshing of 3D models was performed using 10-node tetrahedral elements, which were especially suitable for contact calculations. The linear elements and nodes of each model are shown in Table 2. In all models, the activities of the masticatory muscles were modeled as force

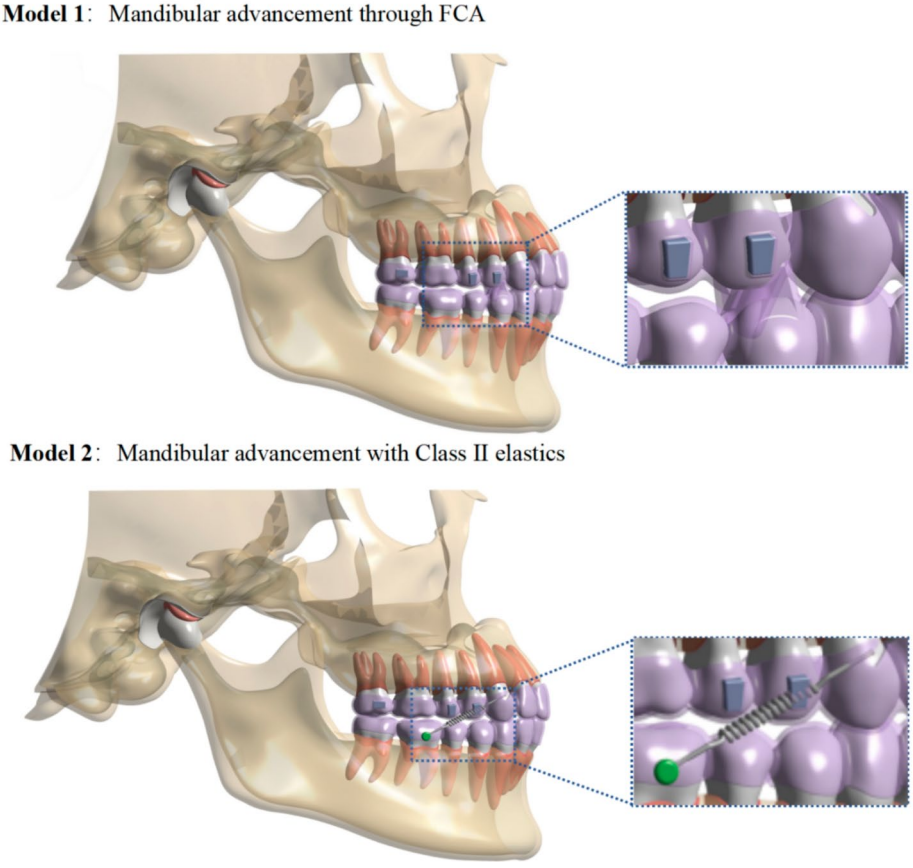

Fig. 3 Two group sets were presented. (**Model 1**) represents using FCA to guide the mandible advancement. FCA was designed with double jaw pads on the clear braces in the upper and lower premolar areas. The angle between the bevels of the jaw pads is 70°; (**Model 2**) simulates using clear aligner combine with Class II elastics. Class II elastics anchored at both ends to the button and precision cutting. The button and precision cutting are located in the buccal of mandibular first molar and maxillary canine, respectively. *FCA*, *Functional clear aligner*

Table 1 Three distinct mesh designs

Designs	Alveolar bone[mm]	PDL [mm]	Attachment[mm]		Teeth[mm]	CA [mm]	Disc [mm]	Cartilage[mm]	Mandibular displacement[mm]	Equivalent stress of the disc (MPa)	Mesh Nodes	Mesh Elements
A	4	0.5	0.5		1	1	1	1	2.9078	0.54256	573,940	310,049
B	4	1	0.5		2	2	1	1	2.9827	0.55495	311,600	165,667
C	4	1.5	0.5		3	3	1	1	2.992	0.55486	272,188	145,185

vectors and spring elements. The distribution and direction of the masticatory muscles are presented schematically in Fig. 5C and D.

Material properties

The biomechanical modeling of the disc was performed using a nonlinear model implemented via an optimized Prony series based on a generalized Maxwell model [9, 12]. The constituent materials of the TMJ except the disc were assumed to be linearly elastic and isotropic. The mechanical properties of the TMJ region are included in Table 3 [12, 14]. Muscle forces in maximum clenching were calculated by multiplying Koolstra's results of the physiologic cross-sectional (PCS) areas by 0.37×10^2 N/m [15–18]. According to the existing literature, the length [16] and PCS [19] area of the masticatory muscle are obtained, and then the Young's modulus and stiffness coefficient of the spring were calculated (Table 4). The force direction [20] of the muscles were presented in Table 5. According to Hooke's law, the muscle forces at different deformations were calculated using the PCS area of the muscles. In previous studies, the muscles were set up as continuously homogenous, isotropic linear elastomers [21]. Because tooth movement was not the primary focus of this study, the periodontal ligament was modeled as a homogeneous layer. The mechanical properties of the other components are detailed in Table 6 [14, 21–23].

Boundary conditions

In terms of boundary conditions, the movement of the maxilla bone was restricted for all degrees of freedom of the nodes at its superior region. Fixed contacts were used between teeth and upper and lower jawbones in order to ensure stable contact without slipping or separation. Non-contact between the clear aligners attached to the maxilla and mandible were also taken into consideration. The bonding contact was set for interfaces of cancellous bone-cortical bone, cortical bone-PDL, PDL-tooth, and tooth-attachment. Further, the connections between the adjacent teeth were assumed to be no separation from their interfaces, however, small amounts of frictionless sliding are allowed to occur along the contact faces. The external surface of the attachments and tooth crown and the internal surface of the aligners were defined as a small-sliding surface-to-surface contact [24] with the friction coefficient set to 0.2 [23, 25]. The friction between the disc and condyle, and between the disc and temporal bone joint surface was minimized by the surrounding synovial fluid with a friction coefficient of 0.001 [26].

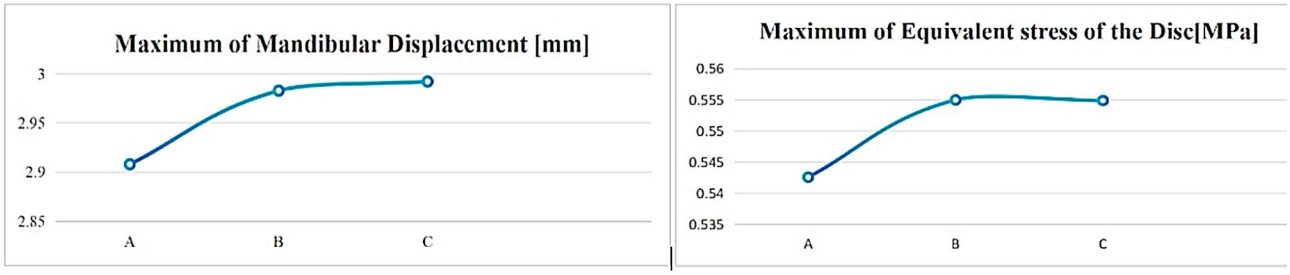

Fig. 4 Convergence analysis of the mesh. The (**A**), (**B**), and (**C**) in the two diagrams represent the following meanings, respectively. **A**:Alveolar bone is 4 mm, the PDL is 0.5 mm, the attachment is 0.5 mm, the tooth is 1 mm, the clear aligner is 1 mm, the disc is 1 mm, and the cartilage is 1 mm.**B**: Alveolar bone is 4 mm, the PDL is 1 mm, the attachment is 0.5 mm, the tooth is 2 mm, the clear aligner is 2 mm, the disc is 1 mm, and the cartilage is 1 mm; **C**: Alveolar bone is 4 mm, the PDL is 1.5 mm, the attachment is 0.5 mm, the tooth is 3 mm, the clear aligner is 3 mm, the disc is 1 mm, and the cartilage is 1 mm

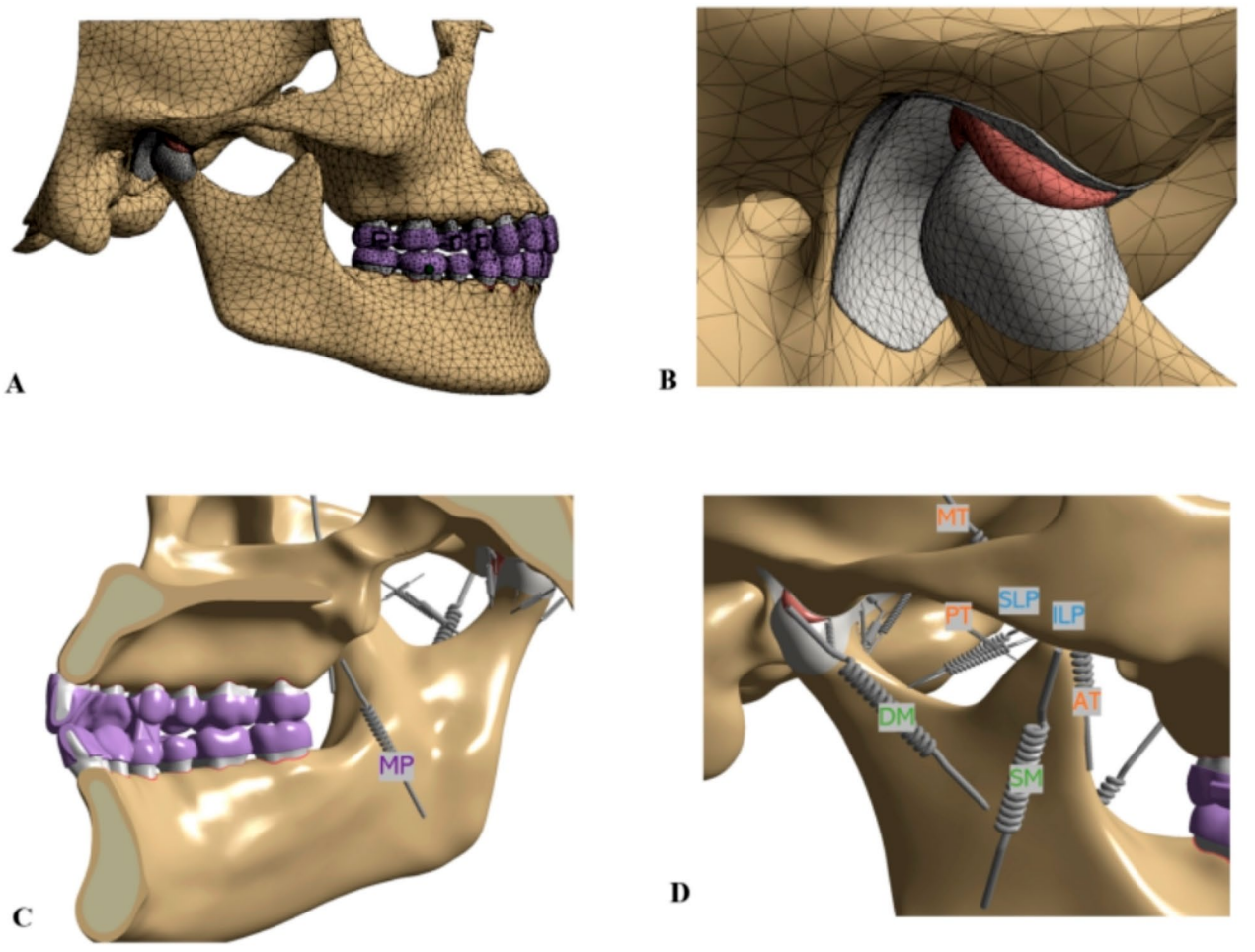

Fig. 5 Mesh configuration. (**A**) The mesh of Maxilla-Mandibular-TMJ-CA; (**B**) The reconstructed detailed anatomical pattern of the TMJ area; (**C**) Medial pterygoid muscle (purple); (**D**) Masseter muscle (green), Temporal muscle (orange), Lateral pterygoid muscle (blue)

Table 2 Nodes and elements

Variables	Nodes	Elements
Model 1	311,600	165,667
Model 2	313,872	165,447

Finite element analysis

Four steps were identified in the appliance-wearing process: 0.025 s, 0.05 s, 0.075 s, and 0.1 s. A retention phase with four stages—25 s, 50 s, 75 s, and 100 s—was added to account for the adaptive changes in muscle tissue that occur after full appliance fitting. To simulate the simplified mandibular advancement process, two models were

Table 3 TMJ region material properties

Model part	Young's modulus[MPa]	Poisson's ratio	Prony series	Relaxation times[s]	Relative modulus
Condylar cartilage [12, 14]	0.8	0.30			
Temporal cartilage [12, 14]	1.5	0.30			
			term 1	0.0384	0.5733
Disc(viscoelasticity) [12, 14]	0.18	0.40	term 2	0.4925	0.1223
			term 3	6.3499	0.0818
			term 4	106.4815	0.0926

Table 4 Young's modulus and stiffness coefficient of masticatory muscle

Masticatory muscles	Length (mm)[16]	PCS ($mm^{2)}$ [19]	E (*N*/mm2)	Stiffness coefficient *N*/mm K = E*A/L
Masseter muscle	23.5	533	0.11	2.494893617
Temporal muscle	35	521	0.11	1.637428571
Medial pterygoid muscle	14.7	370	0.11	2.768707483
Lateral pterygoid muscle	26.9	422	0.11	1.725650558

Table 5 Direction assigned to the masticatory muscles

Muscle	Maximum force (*N*) [15]	Cox-x [20]	Cox-y [20]	Cox-z [20]
SM	190.4	-0.207	-0.419	0.884
DM	81.60	-0.546	-0.358	0.758
AT	158.0	-0.149	-0.044	0.988
MT	95.60	-0.222	0.500	-0.837
PT	75.60	-0.208	0.855	0.474
MP	174.8	0.486	-0.373	0.791
SLP	28.70	0.186	-0.124	-0.037
ILP	66.90	0.178	-0.198	-0.025

Table 6 Material properties of the remaining component

Material	Young's modulus (Mpa)	Poisson's ratio
Cortical bone [14, 21, 23]	1.37×10^{4}	0.26
Cancellous bone [14, 21, 23]	1.37×10^{3}	0.30
Tooth [14, 21, 23]	1.96×10^{4}	0.30
PDL [21, 23]	6.9×10^{-1}	0.45
Clear aligner [14, 21, 23]	5.28×10^{2}	0.306
Attachment [14, 21, 23]	1.25×10^{4}	0.36
Button [14]	1.14×10^{5}	0.35

constructed. The area where the displacement and force are applied in the models were shown in Fig. 6. Model 1 simulated mandibular advancement with FCA, while Model 2 mimiced it with Class II elastics combined with clear aligners. Model 1 employed a novel FCA design, enabling a total mandibular displacement of up to 2 mm in both the forward and downward directions, ultimately achieving a Class I molar relationship. In Model 2, a spring applied 150 g of force, mimicking the action of Class II elastics. The spring's geometry replicates dimensions commonly used in clinical practice [13].

Results

Muscle forces and deformation on masticatory muscles

Figure 7 illustrated the forces induced by the masticatory muscles. Notably, the muscle forces were significantly greater during mandible advancement with FCA compared to Class II elastics. Furthermore, during the process of FCA or Class II elastics insertion (0–0.1 s), the muscles forces rose as the closer the appliances were fully insertion. Later, the muscle forces maintained constant at a certain level after the orthodontic appliance was fully in place (0.1–100 s).

In the masseter muscles, Fig. 7. A, the DM in Model 1 generated a larger muscle force than the SM. While in model 2, the SM produced larger muscle forces than the DM. Furthermore, the SM and DM in Model 1 exhibited more coordinated forces, with both exerting tensile forces. In contrast, Model 2 showed uncoordinated forces between these muscles. Here, the SM produced contractile forces, while the DM generated tensile forces. After maintaining the appliance for 100 s, it was observed that the muscle forces of the DM in Model 1 was 3.1 times greater than that of Model 2.

In the temporal muscles, Fig. 7. B, all bundles of the temporal muscle generated stretching muscle forces in Model 1, facilitating the synchronized functioning of the muscles. In contrast, in Model 2, the PT exerted muscle forces that opposed those of the AT and MT, thereby hindering coordinated muscle stabilization. In Model 1, the PT exhibited the highest muscle forces of 1.816 N, whereas the AT muscle demonstrated the lowest muscle forces of 1.27 N. Contrastingly, in Model 2, the AT attained a maximum muscle forces of 0.506 N, while the PT exhibited the lowest forces of 0.117 N. Muscular force values of AT, MT, and PT were 2.5, 8, and 15.5 times greater in Model 1 than in Model 2, respectively.

Figure 7. C revealed that the MP exerted tensile forces in Model 1 and compressive forces in Model 2. Interestingly, both models exhibited similar force magnitudes for the MP. As illustrated in Fig. 7. D, the lateral pterygoid muscles displayed compressive forces in both Model 1 and Model 2. Notably, the SLP and ILP forces were 3.8 and 4.1 times greater in Model 1 than in Model 2,

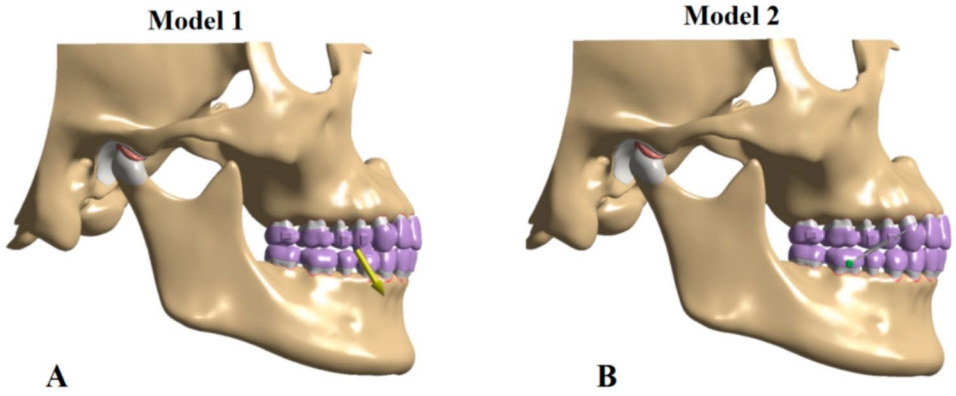

Fig. 6 Boundary condition in the Ansys workbench programme. (**A**): the yellow arrow in Model 1 represented the direction and angle of displacement; (**B**): the spring in Model 2 represented the direction of the force, and the magnitude of the force was 150 g

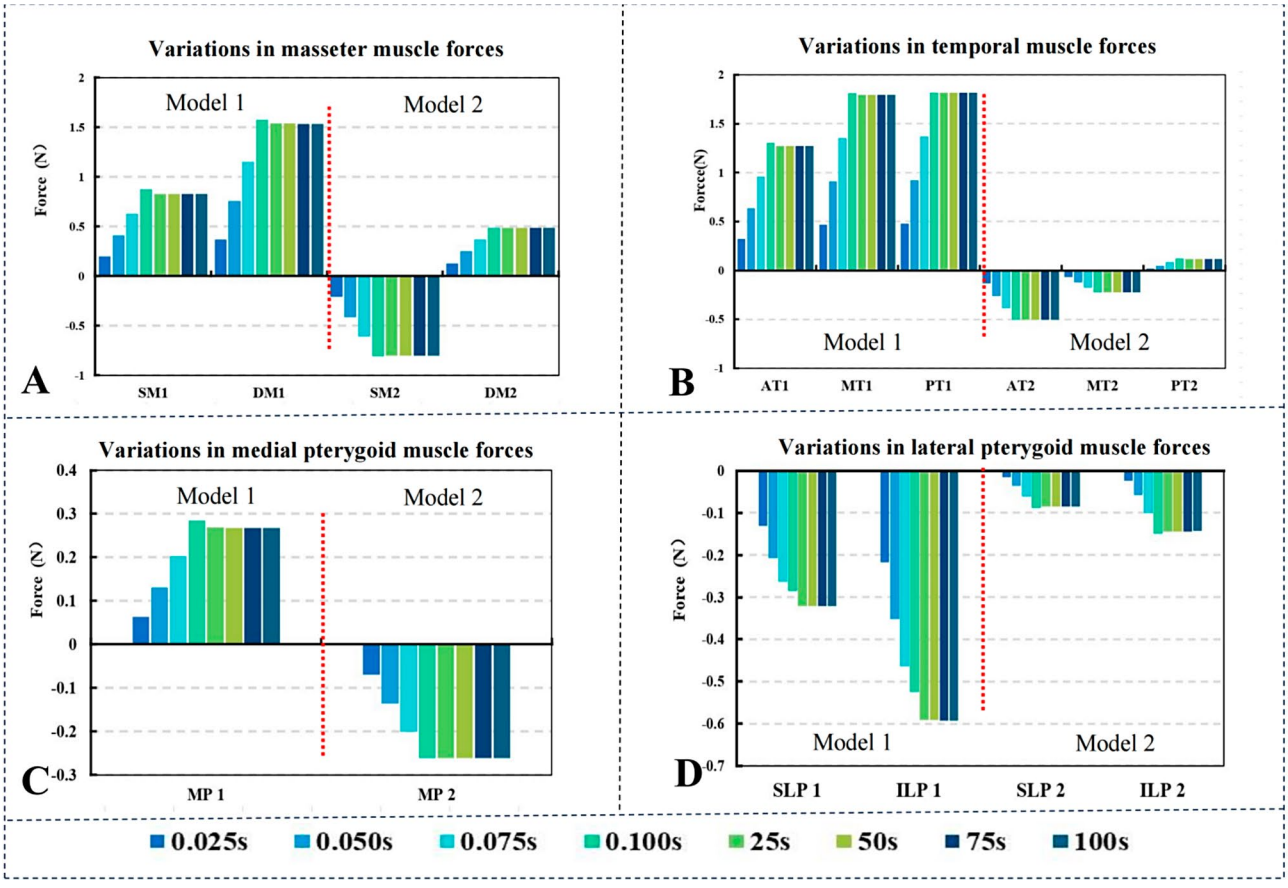

Fig. 7 Masticatory muscles force (N) at 0–100 s during mandibular advancement using FCA or Class II elastics. The legend is situated at the bottom of the entire graph. The red dotted line shows Model 1 data on the left and Model 2 data on the right. (**A**) Trends in the variation of masseter muscle forces; (**B**) Trends in the variation of temporal muscle forces; (**C**) Trends in the variation of medial pterygoid muscle forces; (**D**) Trends in the variation of lateral pterygoid muscle forces

respectively. In Fig. 8, the masticatory muscles deformations were consistent with the magnitude of masticatory muscle forces.

Displacement of the mandible

Figure 9A, B, and C reveal that, in Model 1, at 0.025 s, 0.1 s, and 100 s, the mandible produced a similar displacement tendency, but the displacement at 100 s was 3.5 times greater than that at 0.025 s. Based on the direction of the arrows, the use of FCA to correct Skeletal Class II malocclusion enhanced the forward-downward movement at the mandibular median union and anterior alveolar bone, a tendency for downward movement of the mandibular inferior border, a tendency for forward movement of the mandibular condyles, and a tendency for clockwise rotation of the mandible as a whole. Figure 9D, E, and F reveal that, in Model 2, the mandible also showed a similar displacement trend at 0.025 s, 0.1 s, and 100 s. Interestingly, while the displacement trends for the mandible appeared similar at 0.025 s and 100 s, the displacement at 100 s is 3.75 times greater than the value at 0.025 s. According to the direction of the arrows, the mandibular chin produced a tendency for upward and forward movement with the Class II appliance for Skeletal Class II. In addition, at 100s, the displacement trend of the lower anterior teeth produced in Model 1 was significantly greater than that in Model 2 (Fig. 9C and F).

Stress distribution on the TMJ

Stress distribution on the discs

The maximum equivalent stress on the upper surface of the disc gradually increased with the insertion of the orthodontic appliance, and the stress on the upper surface of the disc reached the highest peak at 0.1 s, with the maximal values of the stress on the upper surface of the disc in Models 1 and 2 reaching 0.626 MPa and 0.0526 MPa, respectively (Fig. 10, A and D). The stress on the upper surface of the disc decreased rapidly in the following 25 s, with decreases of 33.6% and 36.5%, respectively. The stress levels in both models exhibit a slight decrease after this point but then remain largely stable. Notably, the stress on the upper disc surface in Model 1 is roughly eleven times greater than in Model 2 (as shown in Fig. 10). Furthermore, the stress distribution in Model 1 concentrated primarily in the middle and lateral bands of the upper disc surface, while Model 2 exhibited stress concentrated mainly in the posterior band. As shown in Fig. 10B, and F, the maximum equivalent stresses on the lower surface of the disc gradually increased with the insertion of the orthodontic appliance, reaching a peak of 0.555 MPa and 0.0512 MPa, respectively, at 0.1 s. Within the following 25 s, the stresses on the lower surface of the disc decreased rapidly by 46.4% and 39.5%, respectively. Subsequently, the pressure continued to decrease slightly but remained largely stable. At the time of stabilization,

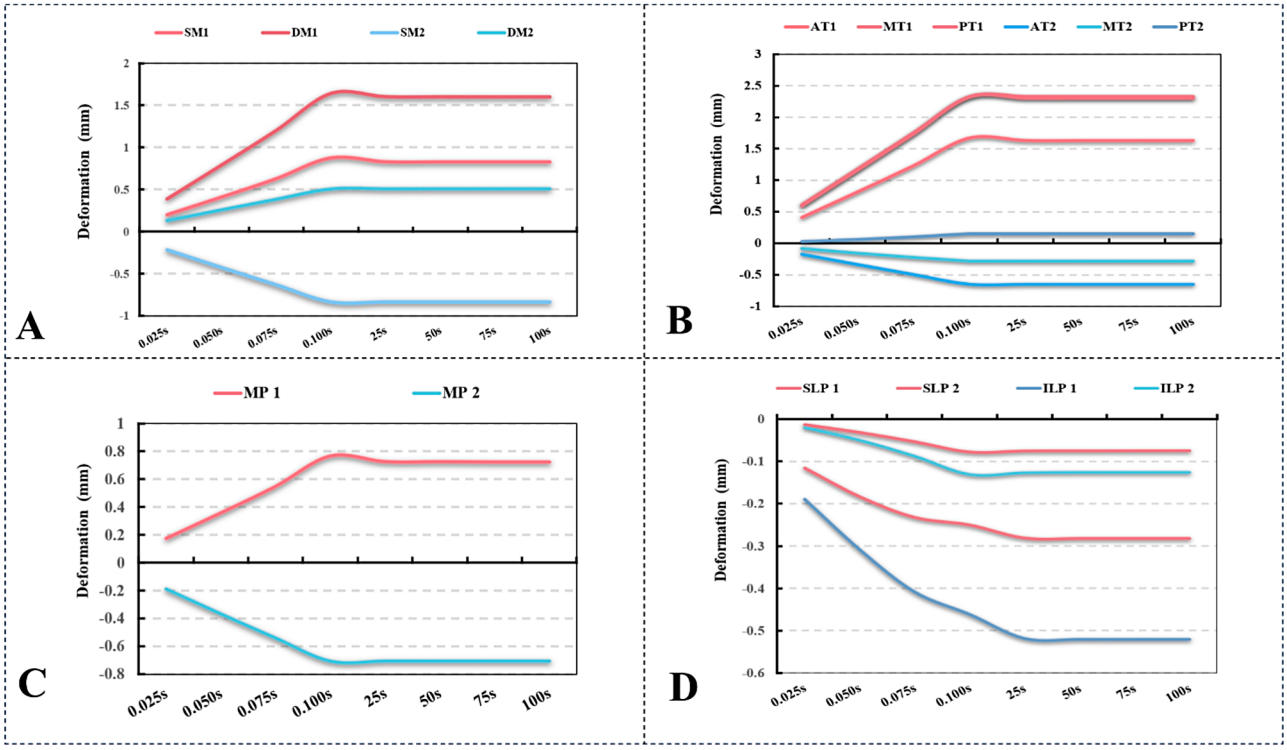

Fig. 8 Deformation of masticatory muscles (mm) at 0–100 s during mandibular advancement using FCA or Class II elastics. (**A**) Masseter muscle; (**B**) Temporal muscle; (**C**) Medial pterygoid muscle forces; (**D**) Lateral pterygoid muscle

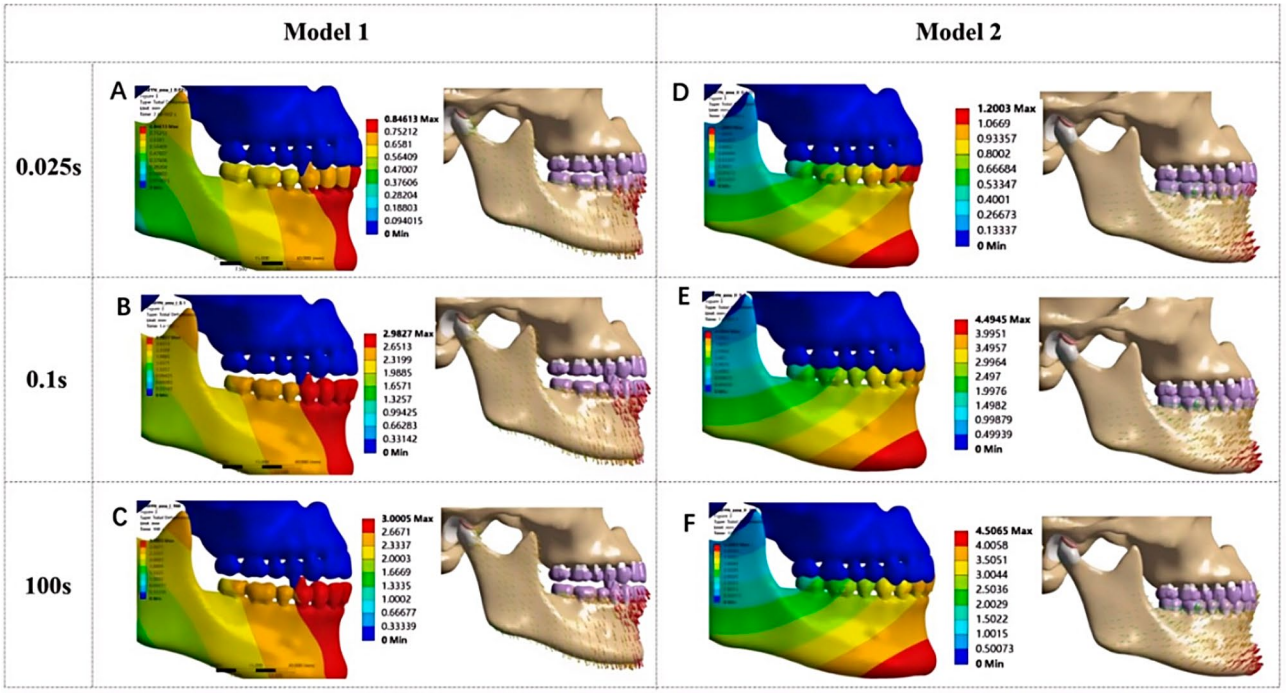

Fig. 9 Displacement of the mandible at 0–100 s during mandibular advancement using FCA or Class II elastics. (**A**), (**B**), and (**C**) represented the displacement trend of the mandible in Model 1 at 0.025s, 0.1s, and 100s, respectively.(**D**), (**E**), and (**F**) represented the displacement trend of the mandible in Model 2 at 0.025s, 0.1s, and 100s, respectively

i.e., 100 s, the stress on the lower surface of the disc in model 1 was about 11 times that in model 2. Figure 11 showed that the stress on the lower surface of the disc in Model 1 was mainly in the middle band, and moved toward the anterior band as the orthodontic appliance was inserted. In Model 2, the stress on the lower surface of the disc was mainly concentrated in the posterior band and moved toward the middle band as the Class II elastics were put on. The upper surface of the disc was slightly more stressed than the lower surface.

Stress distribution on the condyles

Data shown in Fig. 10C and G implyed that the maximum equivalent stress on the condylar gradually increased during mandibular advancement using two methods and reached a maximum of 0.1 s. At this time, the condylar stresses in Model 1 and Model 2 were 0.147 MPa and 0.022 MPa, respectively. During the following 25 s, the stresses decreased by 8.8% and 8.3%, respectively. This is ascribed to the direct contact between the condyle and the disc, which is made of viscoelastic materials.

Figure 11 illustrated that in Model 1, the maximum equivalent force acting on the condylar surface reached 0.033 MPa at 0.025 s. This stress was primarily concentrated in the anterior region of the condyle. Once the appliance was fully seated and worn for 100 s, the maximum equivalent force on the condylar surface increased to 1.335 MPa, which was 40 times greater than the initial value. However, the area of stress concentration remains unchanged. In Model 2, the maximum equivalent force of the condylar surface at 0.025 s was 0.0039 MPa, and the stress concentration area of the condylar surface was mainly in the anterior of the condyle. When the appliance was completely worn in and kept for 100s, the maximum equivalent force of the condylar surface was calculated by 0.01978 MPa, which was 5 times more relative to that of the initial wearing in, but the stress concentration area was not significant. The stress concentration area did not experience significant variation. Figure 10A and B, the posterior part of the condyle was subjected to tensile stress, and the value of tensile stress for Model 1 group was 10 times that of Model 2.

Stress distribution on the glenoid fossa

Results shown in Fig. 10D and H illustrate that the maximum equivalent stress in the glenoid fossa increased gradually with the insertion of two orthodontic appliances. The stress peaked at the time of orthodontic appliances in position (0.1 s). Notably, the stress decreased significantly during the retention phase in the Model 1 group, whereas in Model 2 it was maintained at the level at the peak. As shown in Fig. 11, in Model 1, the maximum equivalent force at the glenoid fossa can be seen at 0.025s to be 0.016 MPa. The stress at the glenoid fossa is a concentrated area mainly in the posterior and medial junctions. By the time the appliance was fully inserted

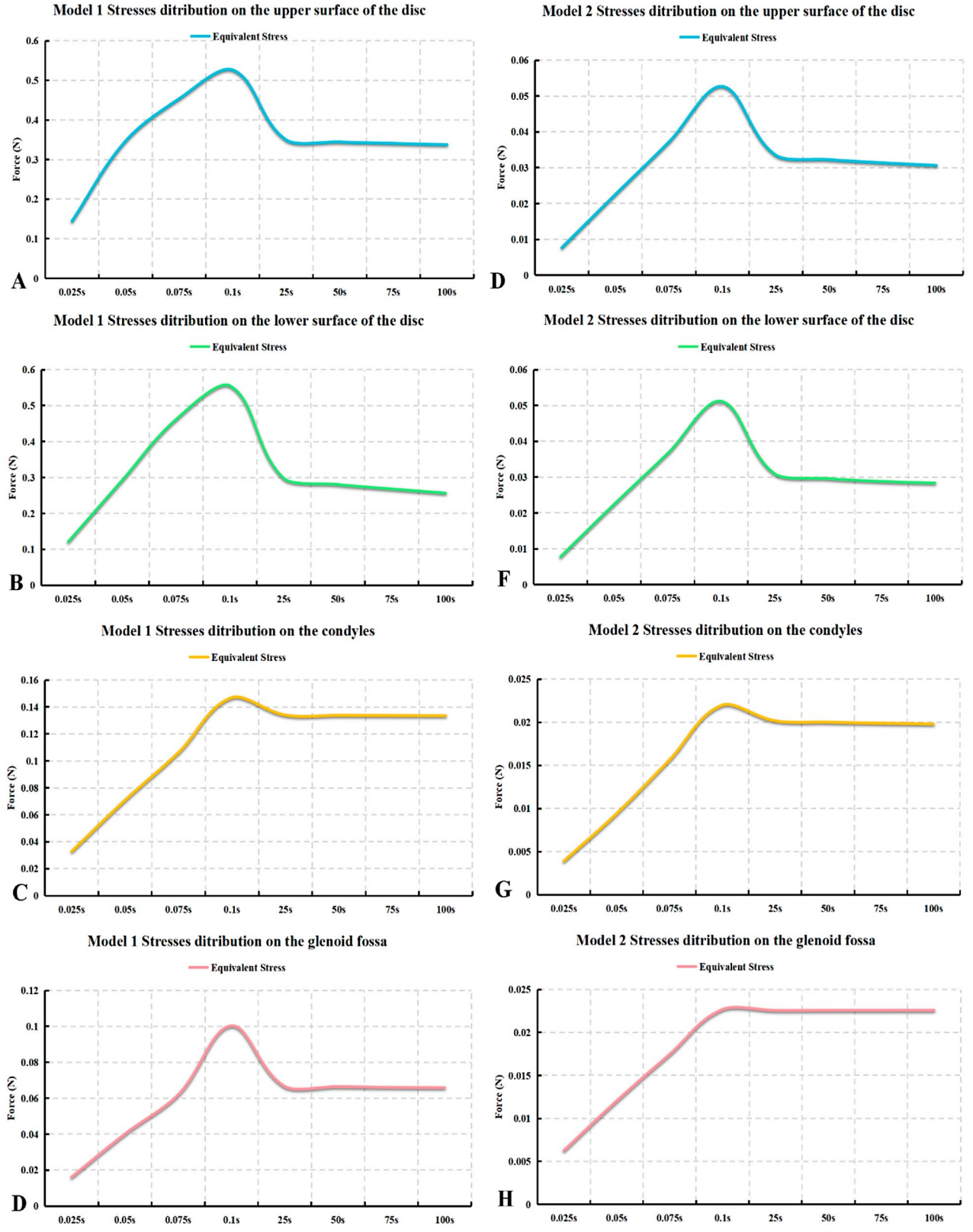

Fig. 10 Stress distribution on the TMJ region at 0–100 s during mandibular advancement using FCA or Class II elastics (MPa). (**A**, **B**, **C**, and **D**) for Model (1) (**E**, **F**, **G**, and **H**) for Model (2) (**A**, **B**, **E**, and **F**) represented disc. (**C** and **G**) represented condyles; (**D** and **H**) represented glenoid fossa

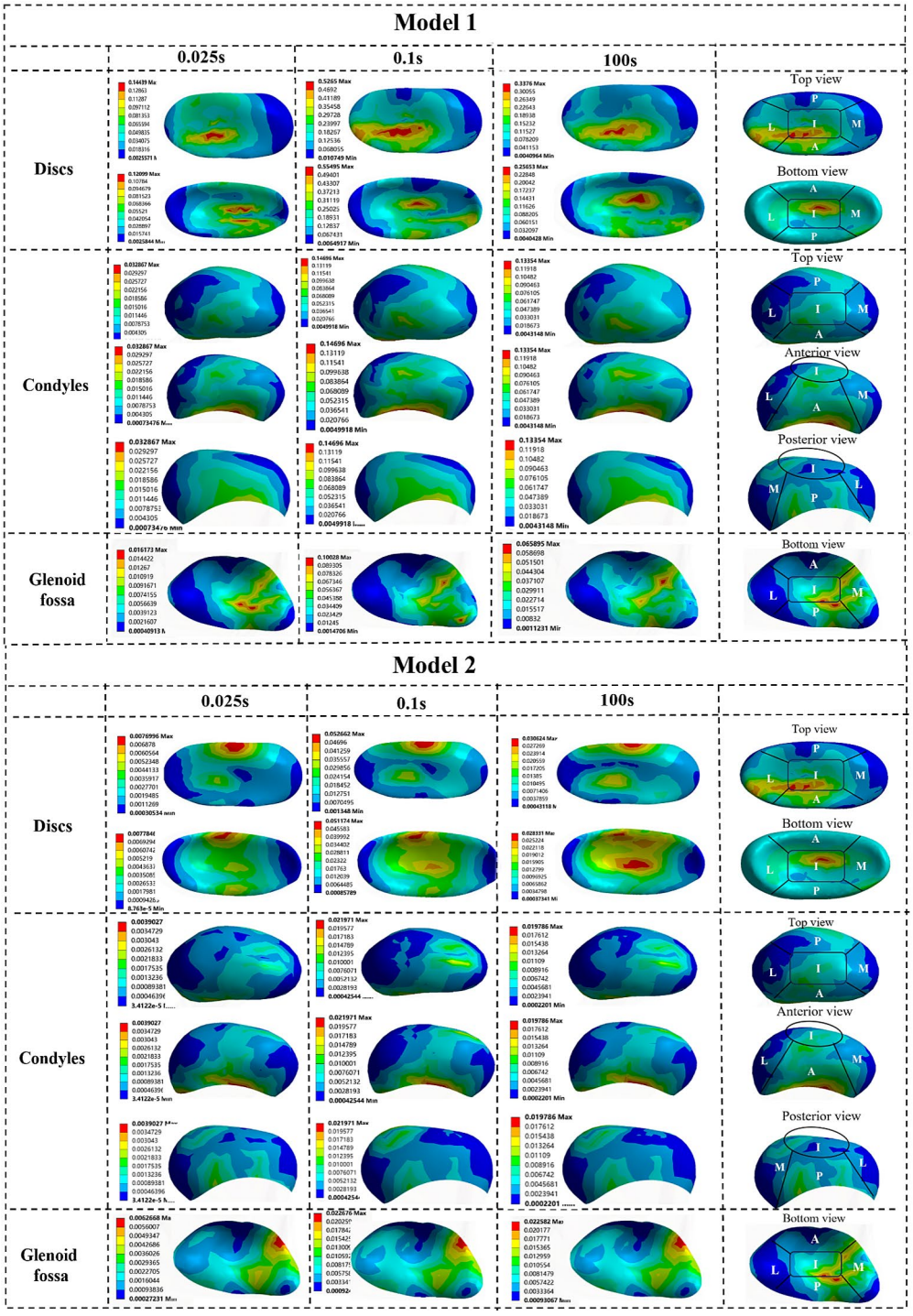

Fig. 11 The equivalent stress distribution on the TMJ region (MPa). **L**: lateral band/ lateral area; **M**: medial band/ medial area; **A**: anterior band/ anterior area; **P**: posterior band/ posterior area; **I**: intermediate band/ intermediate area

and held for 100 s, the maximum equivalent force on the glenoid fossa could be seen to be 0.066 MPa, and the stress was concentrated on the medial and anterior side of the glenoid fossa. In Model 2, the maximum equivalent force on the glenoid fossa reached 0.0063 MPa at 0.025 s. This stress was concentrated on the anterolateral aspect of the fossa. After the appliance was fully seated and worn for 100 s, the maximum equivalent force increased to 0.023 MPa, with stress concentrated in the anteromedial area of the glenoid fossa. The stress increased by 3.6 times during this process.

Figure 12A and B, the posterior portion of the glenoid fossa was subjected to tensile stress, with the tensile stress value for Model 1 being 4.1 times that of Model 2.

Discussion

Functional appliances are often considered the classical treatment for adolescents with Skeletal Class II malocclusion [27]. Similar to traditional functional appliances, FCA is designed with bite blocks or precision wings combined with a clear aligner to reconstruct the neuromuscular balance in the mandibular advancement position and to stimulate bone remodeling in the TMJ region [8, 28]. These changes can correct the sagittal imbalance and improve the facial profile [29]. The stability of the treatment in Skeletal Class II patients is influenced by three factors [30]. The first is the establishment of a new equilibrium of the masticatory muscles in the mandibular anterior position. The second is the adaptive reconstruction of the condyle-glenoid fossa. The third aspect is the vertical eruption of the posterior mandibular teeth to form stable Class I occlusal contact relations. Therefore, studying the biomechanical behavior of masticatory muscles and TMJ is of significant importance for understanding the treatment and recurrence of patients with Skeletal Class II malocclusion. Therefore, in this study, we constructed an innovative 3D finite element model and systematically investigated the effects of using two orthodontic appliances with different principles on the stresses and deformation of the masticatory muscles and TMJ.

Studies have shown that musculature significantly influences facial morphology in the vertical, transverse, and sagittal dimensions. Additionally, researchers have found a link between new bone formation at the condyle and glenoid fossa during mandibular protraction and increased electromyography (EMG) activity in the masseter and temporal muscles [31, 32]. The masseter, temporal, medial pterygoid, and lateral pterygoid muscles attach directly to the mandible and, once activated, pull the mandible to move [18]. Therefore, these four muscles were included in this study. To the best of our knowledge, this is the first study to continuously simulate the changes in masticatory muscle forces and deformation during the orthodontic appliances wearing (0–0.1 s) and holding stages (0.1–100 s).

The study observed a gradual increase in masticatory muscle force with both orthodontic appliance insertion and progressive mandibular advancement. Following initial placement, there was a slight decrease in muscle force between 0.1 and 0.25 s, before stabilizing at an activation level. This is related to the use of viscoelastic materials for modeling the articular discs in this study. The phenomenon of relaxation is produced in a viscoelastic material when it is subjected to a constant strain [33]. In addition, the value of the masticatory muscle force of the mandible advancement using FCA was significantly greater than that of the mandible advancement mode using Class II elastics, this suggested that the FCA can produce greater muscle forces on the jawbones at its muscle attachments. This difference likely stems from the greater degree of

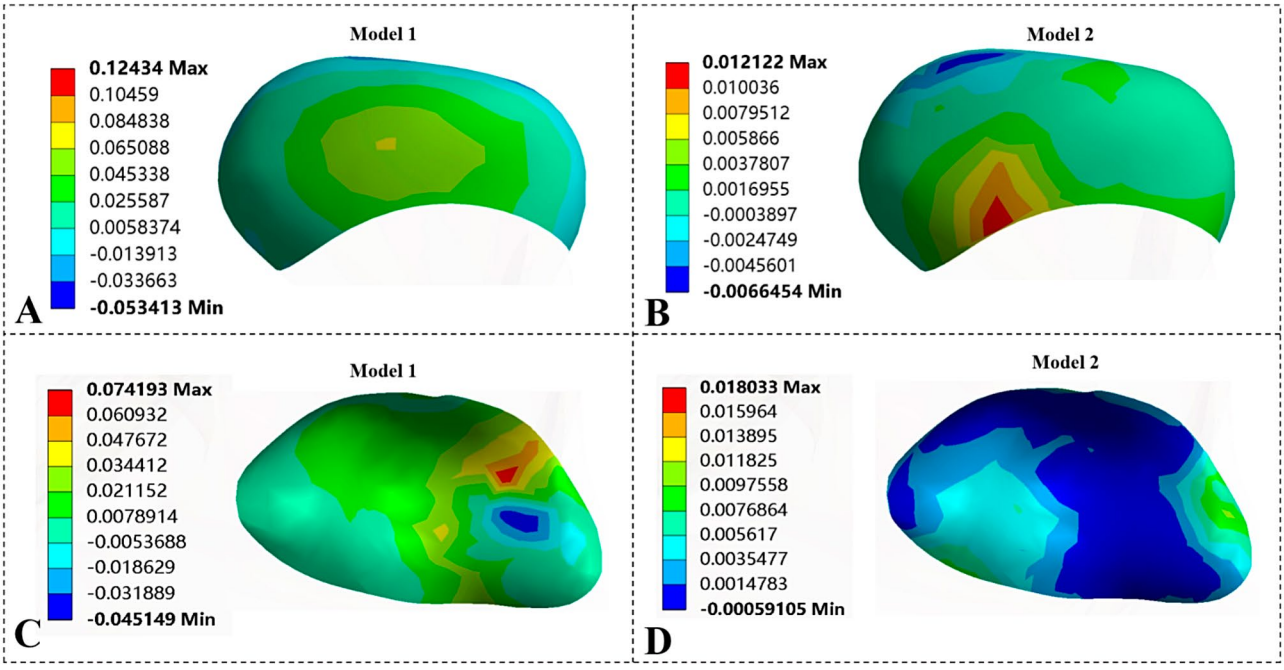

Fig. 12 The maximum principle stress distribution on the posterior view of the condylar (**A** and **B**), and the bottom view of the glenoid fossa (**C** and **D**)

anterior mandibular displacement produced by the FCA's mechanical lock compared to the limited displacement achieved by Class II elastics. In previous studies, both class II elastics and functional appliances contributed to the correction of malocclusions by skeletal and dental changes, but class II elastics had a greater impact on dentoalveolar changes [30].

According to anatomy, the main role of the masseter muscles is to lift the mandible upward and chew foods, and the contraction of the SM can make the mandible slightly extend forward [34]. The FCA model appeared to contribute to mandibular relapse after treatment. During wear, the SM applied a stretching force that pulls the jaw backward. Conversely, the Class II elastics model helped maintain a stable jaw position following correction. In this model, the SM muscle exerts a compressive force that pulls the jaw forward. This suggests to the orthodontist that after using FCA to correct skeletal deformities, Class II elastics can be used to promote the establishment of masticatory muscle balance while maintaining orthodontic results.

Temporal muscles — as the largest of the masticatory muscles in terms of area and volume — have a great influence on the function of the maxillofacial masticatory system [35]. The temporal muscle is fan-shaped and can be divided into three parts, The muscle fibers of the AT are vertically downward, those of the MT are oriented forward and downward, and those of the PT are oriented forward [36]. In Model 1, the combined action of the AT and MT tends to rotate the mandible forward and clockwise. This rotation is unfavorable for orthodontic treatment in Class II hyperdivergent patients because it can worsen their facial profile. Conversely, in Model 2, the AT and MT work together to rotate the mandible forward and counterclockwise. It is a more suitable choice for Class II hyperdivergent patients. The PT muscle was directly related to the sagittal movement of the mandible, pulling the mandible backward when the posterior fascicle of the temporal muscle contracted. The muscle tensile strength of the PT in Model 1 was 15.5 times higher than that of Model 2. This further confirmed that FCA produced a better mandibular advancement effect.

Studies have demonstrated that the deformation of the MP was affected by the position and length of the mandible [37]. The MP primarily lifts the mandible upwards. In the FCA group, it exerted tensile forces that pulled the mandible downward. Conversely, in the Class II elastics model, it produced compressive forces that pulled the mandible upward. This suggests that FCA was not ideal for Class II hyperdivergent patients. Proponents of FCA argue that the full-wrap design effectively prevents posterior elongation compared to traditional functional appliances, leading to better vertical control of the back teeth. The results of a prospective clinical study showed an increase in the length of the internal pterygoid and masseter muscles after wearing functional appliances for half a year [38], validating the trend of the internal pterygoid and masseter muscles after using FCA in our study. The lateral pterygoid muscles played a unique role in jaw movement control due to their attachment to both the temporomandibular disc and condyle [39]. In terms of mandibular movement function, the lateral pterygoid muscle mainly controls the horizontal movement of the mandible [40]. It also regulated the contraction of the SLP and ILP during mandibular advancement with both orthodontic appliances which as similar to the results reported previously [41].

For the evaluation of the functional status of the masticatory muscles, in addition to the change in muscle forces magnitude, the coordinated movement between the masticatory muscles is also one of the main indicators [42, 43]. Coordinated movements in the masticatory muscles involve synergy not only between left and right homonymous muscles but also between different muscle layers. In the FCA model, various muscle layers contract or stretch uniformly, promoting coordinated and stable muscle forces. This, in turn, contributes to synergistic intermuscular movements. Conversely, the Class II elastic model exhibits opposing actions between distinct layers of the masseter and temporal muscles. These opposing movements hinder the overall contraction of the muscles themselves.

The FCA model caused slight forward tilting and inward tilting of the lower front teeth, especially in patients with thin cortical plates. This is because the aligners act as an overlay and do not provide enough support. In addition, the mechanical interlocking in the FCA model transmits the anterior mandibular force along the appliance, potentially increasing the risk of bone defects like fenestration and dehiscence in these patients. The risk of root resorption and bone defects can be minimized by designing a void in the anterior region to create a stress interruption effect or by utilizing the Micro-screw Implant Anchorage (MIA) for anchorage reinforcement support to control the torque of the lower anterior teeth.

In order to study the stress in the TMJ region, this experiment innovatively adopted viscoelastic material to model the articular disc. Viscoelastic materials exhibit stress relaxation, creep, and hysteresis. This implies they undergo an initial elastic deformation upon force application, followed by time-dependent viscous deformation. These properties allow them to realistically simulate the structure and behavior of the natural articular disc. Wu (2014) postulated that sustained mechanical loading can significantly reduce nutrient levels within the disc, potentially leading to cell death [44]. The results of this study showed that the stresses on the upper and lower surfaces

of the articular disc increased gradually during mandibular advancement using both appliances, and the equivalent stress values reached a peak when the appliance was completed. Following appliance insertion, the articular disc underwent stress relaxation during the retention phase. This resulted in a decrease in stress on the upper surface of the disc by 46.4% and 39.5% for Models 1 and 2, respectively. The stress on the lower disc surface also decreased, but to a lesser extent, with reductions of 8.8% and 8.3% in Models 1 and 2, respectively. Although the material properties of the temporal bone fossa and condyle were linear in this study, a certain degree of stress relaxation also occurred during the retention phase after the appliance was inserted, probably because the articular disk was between the temporal bone fossa and condyle and acted as a stress buffer. A comparison of Model 1 and Model 2 revealed that the equivalent stresses in the articular discs were significantly higher in Model 1. This is related to the fact that the mechanical inlay structure produces a stronger force of mandibular anterior displacement than Class II elastics traction.

Condylar chondrocytes are mechanically sensitive. The equivalent stress represents the comprehensive stress value, and exploring the equivalent stress that occurs on the condyle is helpful in finding the stress concentration area. In laboratory experiments, condylar chondrocytes can differentiate more rapidly when subjected to pressure relief in the posterior condyle, away from the glenoid fossa. This pressure on the condyle triggers neovascularization and osteogenesis in the back of the condyle, ultimately causing the condyle to adapt and grow. Studies on animals also have shown this effect [45–47]. Since the maximum principal stress reflects tensile stress, which promotes new bone formation, we further analyzed the maximum principal stress in this region. In this study, the posterior aspect of the condyle and glenoid fossa generated tensile stress when FCA or Class II elastics were employed, the tensile stress generated by the FCA model was highly pronounced, which established a favorable growth environment for chondrocytes, making them differentiate. This increases the formation of new bone in the posterior part of the condyle and glenoid fossa, thereby promoting mandibular advancement, consistent with a previous study [30].

Different orthodontic treatments are suitable for different skeletal facial types. In general, FCA is better for adolescent skeletal class II patients with low-angle facial and developed masticatory muscles, while Class II elastics traction is more suitable for those with high-angle facial and underdeveloped masticatory muscles. Besides, Class II traction can be used to maintain treatment effects in later orthodontic phases for patients initially treated with FCA. Regardless of the techniques used for mandibular advancement, it can cause lower anterior teeth lip tilt, potentially increasing the risk of bony dehiscences and fenestrations. This requires orthodontists' attention. Additionally, there will be significant stress in the TMJ areas during the process, necessitating close clinical monitoring and possibly CBCT.

Although the FEA technology has been widely applied in biomechanical analysis with good results, some limitations need to be considered. Given that the finite element model was constructed using data from one patient, the results may be biased and need to be validated in larger samples. TMJ morphology variations could also have an effect on the results. Muscle adaptation is a slow process, and while FEA can predict short-term changes and trends, the long-term effects on the masticatory muscles remain unclear and require further investigation. Moreover, bone and muscle are not uniform materials. Their properties, such as Young's modulus and Poisson's ratio, vary across different regions and ages. Future research should account for this heterogeneity for more accurate modeling.

Conclusion

1. The FCA model generated stronger and more coordinated masticatory muscle forces compared to the Class II elastics model.
2. There was a tendency for forward-downward displacement of the anterior mandible in the FCA model, whereas there was a tendency for forward-upward displacement in the Class II elastics model.
3. The location and magnitude of intra-articular stresses generated by the two types of appliances were different. The articular disc cushioned some of the stress and reduced intra-articular stress.
4. The FCA model produced higher tensile stress on the condyle and the posterior part of the articular fossa than the Class II elastics model, which contributed to the formation of a new bone.

Abbreviations

FCA	Functional Clear Aligner.
FEA	Finite element analysis.
SM	Superficial masseter muscle.
DM	Deep masseter muscle.
AT	Anterior temporal muscle.
MT	Medial temporal muscle.
PT	Posterior temporal muscle.
MP	Medial pterygoid.
SLP	Superior lateral pterygoid muscle.
ILP	Inferior lateral pterygoid muscle.
TMJ	Temporomandibular joint.

Acknowledgements

The authors would like to express their gratitude to EditSprings (https://www.editsprings.cn) for the expert linguistic services provided.

Author contributions
Mingxin Zhang and Xulin Liu: Data collection and analysis, Article writing; Ruijie Zhang: Methodology, Software; Xin Chen and Zhixin Song: Data collection and analysis; Yanning Ma: Funding acquisition, Manuscript review; Zuolin Jin: Funding acquisition, Supervision, Manuscript review.

Funding
This work was supported by the National Clinical Research Center for Oral Disease(LCA202202, LCB202202); Key Research and Development Program of Shaanxi Province (2021SF-050, 2022SF-227); the CSA Clinical Research Fund (CSA-02022-01); College Science and Technology Innovation Plan of Shanxi Education Department (2021L242); New Technologies and New Business of School of Stomatology, Air Force Medical University Fund (LX2022-401); China Oral Health Foundation (A2023-019).

Data availability
The datasets used or analyzed during the current study are available from the corresponding author on reasonable request.

Declarations

Ethics approval and consent to participate
This study was approved by the Ethics Committee of The Air Force Medical University (IRB: KQ-YJ-2024-012). All methods were carried out in accordance with relevant guidelines and regulations. Informed consent was obtained from all participants and/or their legal guardian(s).

Consent for publication
Not applicable.

Competing interests
The authors declare no competing interests.

Author details
[1]State Key Laboratory of Oral & Maxillofacial Reconstruction and Regeneration, National Clinical Research Center for Oral Diseases, Shaanxi Clinical Research Center for Oral Diseases, Department of Orthodontics, School of Stomatology, Air Force Medical University, Xi'an 710032, China

Received: 21 May 2024 / Accepted: 24 October 2024
Published online: 29 October 2024

References

1. Ding L, Chen R, Liu J, Wang Y, Chang Q, Ren L. The Effect of Functional Mandibular Advancement for adolescent patients with skeletal class II malocclusion on the tmj: a systematic review and Meta-analysis. BMC Oral Health. 2022;22:51. https://doi.org/10.1186/s12903-022-02075-8.
2. McNamara JJ. Components of class II malocclusion in children 8–10 years of age. Angle Orthod. 1981;51:177–202. https://doi.org/10.1043/0003-3219(1981)051%3C0177:COCIMI%3E2.0.CO;2.
3. Zreaqat M, Hassan R, Samsudin AR, Alforaidi S. Effects of twin-block appliance on upper airway parameters in Osa children with class II malocclusion and mandibular retrognathia: a Cbct study. Eur J Pediatr. 2023;182:5501–10. https://doi.org/10.1007/s00431-023-05226-3.
4. Zhou L, Wang YM, Zhang L, Yao J. Functional clear aligner treatment of class II malocclusion in teenagers [Hua Xi, Kou Qiang, Yi Xue, Za Zhi]. 2019;37:236–41. https://doi.org/10.7518/hxkq.2019.03.002.
5. Janson G, Sathler R, Fernandes TM, Branco NC, Freitas MR. Correction of class II malocclusion with class II elastics: a systematic review. Am J Orthod Dentofac. 2013;143:383–92. https://doi.org/10.1016/j.ajodo.2012.10.015.
6. Murakami K, Yamamoto K, Kawakami M, Horita S, Kirita T. Changes in strain energy density in the temporomandibular joint disk after sagittal split ramus osteotomy using a computed tomography-based finite element model. J Orofac Orthop. 2024;85:289–305. https://doi.org/10.1007/s00056-022-00441-3.
7. Lai L, Huang C, Zhou F, Xia F, Xiong G. Finite elements analysis of the temporomandibular joint disc in patients with intra-articular disorders. BMC Oral Health. 2020;20:93. https://doi.org/10.1186/s12903-020-01074-x.
8. Zhu C, Li R, Yuan L, Zheng Y, Jin Y, Li H, Liu C, Xia L, Fang B. Effects of the advanced mandibular spring on mandibular retrognathia treatment: a three-dimensional finite element study. BMC Oral Health. 2022;22:271. https://doi.org/10.1186/s12903-022-02308-w.
9. Barrientos EFAL. Optimal discrete-time prony series fitting method for viscoelastic materials. Mech Time Depend Mat. 2019;23:193–206. https://doi.org/10.1007/s11043-018-9394-z.
10. Duggal I, Singh N, Tripathi T. Queries regarding clinical finite element analysis of mandibular displacement model treated with twin-block appliance. Am J Orthod Dentofac. 2023;164:461–2. https://doi.org/10.1016/j.ajodo.2023.06.019.
11. Ortun-Terrazas J, Cegonino J, Perez DPA. Biomechanical impact of the porous-fibrous tissue behaviour in the temporomandibular joint movements. An in silico approach. J Mech Behav Biomed. 2021;120:104542. https://doi.org/10.1016/j.jmbbm.2021.104542.
12. Barrientos E, Pelayo F, Tanaka E, Lamela-Rey MJ, Fernandez-Canteli A, de Vicente JC. Effects of loading direction in prolonged clenching on stress distribution in the temporomandibular joint. J Mech Behav Biomed. 2020;112:104029. https://doi.org/10.1016/j.jmbbm.2020.104029.
13. Liu X, Wang W, Gao J, Qin W, Wen Y, Luo H, Ma Y, Jin Z. Actual contribution ratio of maxillary and mandibular molars for total molar relationship correction during maxillary molar sequential distalization using clear aligners with class II elastics: a finite element analysis. Am J Orthod Dentofac. 2023;164:e106–20. https://doi.org/10.1016/j.ajodo.2023.07.007.
14. Liu X, Cheng Y, Qin W, Fang S, Wang W, Ma Y, Jin Z. Effects of upper-molar distalization using clear aligners in combination with class II elastics: a three-dimensional finite element analysis. BMC Oral Health. 2022;22:546. https://doi.org/10.1186/s12903-022-02526-2.
15. Gao W, Lu J, Gao X, Zhou J, Dai H, Sun M, Xu J. Biomechanical effects of joint disc perforation on the temporomandibular joint: a 3D finite element study. BMC Oral Health. 2023;23:943. https://doi.org/10.1186/s12903-023-03521-x.
16. Weijs WA, Hillen B. Relationship between the physiological cross-section of the human jaw muscles and their cross-sectional area in computer tomograms. Acta Anat (Basel). 1984;118:129–38. https://doi.org/10.1159/000145832.
17. Koolstra JH, van Eijden TM. Application and validation of a three-dimensional mathematical model of the human masticatory system in vivo. J Biomech. 1992;25:175–87. https://doi.org/10.1016/0021-9290(92)90274-5.
18. Duggal I, Sidhu MS, Chawla A, Dabas A, Dhimole VK. Effects of miniplate anchored herbst appliance on skeletal, dental and masticatory structures of the craniomandibular apparatus: a finite element study. Int Orthod. 2021;19:301–9. https://doi.org/10.1016/j.ortho.2021.04.002.
19. Weijs WA, Hillen B. Physiological cross-section of the human jaw muscles. Acta Anat (Basel). 1985;121:31–5. https://doi.org/10.1159/000145938.
20. Chen X, Wang Y, Mao Y, et al. Biomechanical evaluation of Chinese customized three-dimensionally printed total temporomandibular joint prostheses: a finite element analysis. J Cranio Maxill Surg. 2018;46:1561–8. https://doi.org/10.1016/j.jcms.2018.06.018.
21. Ma Y, Li S. The optimal orthodontic displacement of clear aligner for mild, moderate and severe periodontal conditions: an in vitro study in a periodontally compromised individual using the finite element model. BMC Oral Health. 2021;21:109. https://doi.org/10.1186/s12903-021-01474-7.
22. Chabanas M, Luboz V, Payan Y. Patient specific finite element model of the face soft tissues for computer-assisted maxillofacial surgery. Med Image Anal. 2003;7:131–51. https://doi.org/10.1016/s1361-8415(02)00108-1.
23. Cheng Y, Gao J, Fang S, Wang W, Ma Y, Jin Z. Torque movement of the upper anterior teeth using a clear aligner in cases of extraction: a finite element study. Prog Orthod. 2022;23:26. https://doi.org/10.1186/s40510-022-00421-8.
24. Liu L, He B, Zhuang J, Zhang L, Lv A. Force measurement system for invisalign based on thin film single force sensor. Measurement. 2017;97:1–7.
25. Gomez JP, Pena FM, Martinez V, Giraldo DC, Cardona CI. Initial force systems during bodily tooth movement with plastic aligners and composite attachments: a three-dimensional finite element analysis. Angle Orthod. 2015;85:454–60. https://doi.org/10.2319/050714-330.1.
26. Tanaka E, Pelayo F, Kim N, Lamela MJ, Kawai N, Fernandez-Canteli A. Stress relaxation behaviors of articular cartilages in porcine temporomandibular joint. J Biomech. 2014;47:1582–7. https://doi.org/10.1016/j.jbiomech.2014.03.007.
27. Pancherz H, Malmgren O, Hagg U, Omblus J, Hansen K. Class II Correction in herbst and bass therapy. Eur J Orthodont. 1989;11:17–30. https://doi.org/10.1093/oxfordjournals.ejo.a035960.

28. Zhang Y, Zheng X, Zhang Q, He Z, Huang W, Yan X, Lv T, Yuan X. Clinical finite element analysis of mandibular displacement model treated with twin-block appliance. Am J Orthod Dentofac. 2023;164:395–405. https://doi.org/10.1016/j.ajodo.2023.02.012.
29. Elfeky HY, Fayed MS, Alhammadi MS, Soliman S, El BD. Three-dimensional skeletal, dentoalveolar and temporomandibular joint changes produced by twin block functional appliance. J Orofac Orthop. 2018;79:245–58. https://doi.org/10.1007/s00056-018-0137-1.
30. Huang W, Dong L, Yu S, et al. Stress distribution of the modified clear twin-block aligner on the temporomandibular joint, alveolar bone and teeth: a finite element analysis. Int Orthod. 2023;21:100815. https://doi.org/10.1016/j.ortho.2023.100815.
31. Smaglyuk LV, Liakhovska AV. Emg-characteristic of masticatory muscles in patients with class II malocclusion and temporomandibular disorders. Wiad Lek. 2019;72:1043–7.
32. Xie J, Huang C, Yin K, Park J, Xu Y. Effects of Orthodontic treatment with activator appliance on patients with skeletal class ii malocclusion: a systematic review and meta-analysis. Ann Palliat Med. 2021;10:12319–34. https://doi.org/10.21037/apm-21-3205.
33. Barrientos E, Pelayo F, Noriega Á, Lamela MJ, Fernández-Canteli A, Tanaka E. Optimal discrete-time prony series fitting method for viscoelastic materials. Mech Time-Depend Mat. 2019; 23:193–206. https://doi.org/10.1007/s11043-018-9394-z
34. Ispir NG, Toraman M. The relationship of masseter muscle thickness with face morphology and parafunctional habits: an ultrasound study. Dentomaxillofac Rad. 2022;51:20220166. https://doi.org/10.1259/dmfr.20220166.
35. Akita K, Fukino K. The significance and classification of the layered structures of the human masseter and temporalis. Ann Anat. 2022;242:151907. https://doi.org/10.1016/j.aanat.2022.151907.
36. Gaudy JF, Zouaoui A, Bravetti P, Charrier JL, Laison F. Functional anatomy of the human temporal muscle. Surg Radiol Anat. 2001;23:389–98. https://doi.org/10.1007/s00276-001-0389-z.
37. Agrawal A, Kumar V, Pillai AR. Contribution of masticatory muscle pattern to craniofacial morphology in normal adults: a cross-sectional Mri study. Natl J Maxillofac Surg. 2023;14:213–20. https://doi.org/10.4103/njms.njms_473_21.
38. Cesur E, Ozdiler O, Koklu A, Orhan K, Seki U. Effects of wear time differences of removable functional appliances in class II patients: prospective Mri study of Tmj and masticatory muscle changes. Oral Radiol. 2020;36:47–59. https://doi.org/10.1007/s11282-019-00379-0.
39. Murray GM, Phanachet I, Uchida S, Whittle T. The role of the human lateral pterygoid muscle in the control of horizontal jaw movements. J Orofac Pain. 2001;15:279–92.
40. Klineberg I. The lateral pterygoid muscle: some anatomical, physiological and clinical considerations. Ann R Australas Coll Dent Surg. 1991;11:96–108.
41. Hiyama S, Ono PT, Ishiwata Y, Kuroda T, McNamara JJ. Neuromuscular and skeletal adaptations following mandibular forward positioning induced by the herbst appliance. Angle Orthod. 2000;70:442–53. https://doi.org/10.1043/0003-3219(2000)070%3C0442:NASAFM%3E2.0.CO;2.
42. Falardeau D, Dubois S, Kolta A. The coordination of chewing. Curr Opin Neurobiol. 2023;83:102805. https://doi.org/10.1016/j.conb.2023.102805.
43. Angst L, Koolstra JH, Wiedemeier D, Van Sluijs RM, Pulfer AM, Gallo LM, Colombo V. Masticatory muscles activation and Tmj space during asymmetrically loaded jaw closing. Ann Biomed Eng. 2024;52:877–87. https://doi.org/10.1007/s10439-023-03424-6.
44. Wu Y, Cisewski SE, Coombs MC, et al. Effect of sustained joint loading on Tmj disc nutrient environment. J Dent Res. 2019;98:888–95. https://doi.org/10.1177/0022034519851044.
45. Xiong H, Rabie AB, Hagg U. Mechanical strain leads to condylar growth in adult rats. Front Biosci. 2005;10:67–73. https://doi.org/10.2741/1507.
46. Xiong H, Rabie AB, Hagg U. Neovascularization and mandibular condylar bone remodeling in adult rats under mechanical strain. Front Biosci. 2005;10:74–82. https://doi.org/10.2741/1508.
47. Rabie AB, Xiong H, Hagg U. Forward mandibular positioning enhances condylar adaptation in adult rats. Eur J Orthodont. 2004;26:353–8. https://doi.org/10.1093/ejo/26.4.353.

Publisher's note